NO Binding and Dynamics in Reduced Heme−Copper Oxidases aa_3 from *Paracoccus denitrificans* and ba_3 from *Thermus thermophilus*[†]

Eric Pilet,[‡] Wolfgang Nitschke,[§] Fabrice Rappaport,[||] Tewfik Soulimane,[⊥] Jean-Christophe Lambry,[‡] Ursula Liebl,[‡] and Marten H. Vos*[,‡]

Laboratory for Optical Biosciences, INSERM U451, CNRS UMR 7645, Ecole Polytechnique-ENSTA, 91128 Palaiseau Cedex, France, Laboratoire de Bioénergétique et Ingéniérie des Protéines UPR 9036, Institut de Biologie Structurale et Microbiologie, CNRS, 31, Chemin Joseph Aiguier, 13402 Marseille, Cedex 20, France, Institut de Biologie Physico-Chimique, CNRS UPR 1261, 13 rue Pierre et Marie Curie, 75005 Paris, France, and Paul Scherrer Institute, Life Sciences, OSRA/008, CH-5232 Villigen PSI, Switzerland

Received June 1, 2004; Revised Manuscript Received July 30, 2004

ABSTRACT: Cytochrome *c* oxidase (C*c*O) has a high affinity for nitric oxide (NO), a property involved in the regulation of respiration. It has been shown that the recombination kinetics of photolyzed NO with reduced C*c*O from *Paracoccus denitrificans* on the picosecond time scale depend strongly on the NO/enzyme stoichiometry and inferred that more than one NO can be accommodated by the active site, already at mildly suprastoichiometric NO concentrations. We have largely extended these studies by monitoring rebinding dynamics from the picosecond to the microsecond time scale, by performing parallel steady-state low-temperature electron paramagnetic resonance (EPR) characterizations on samples prepared similarly as for the optical experiments and comparing them with molecular-modeling results. A comparative study was performed on C*c*O ba_3 from *Thermus thermophilus*, where two NO molecules cannot be copresent in the active site in the steady state because of its NO reductase activity. The kinetic results allow discrimination between different models of NO-dependent recombination and show that the overall NO escape probability out of the protein is high when only one NO is bound to C*c*O aa_3, whereas strong rebinding on the 15-ns time scale was observed for C*c*O ba_3. The EPR characterizations show similar results for aa_3 at substoichiometric NO/enzyme ratios and for ba_3, indicating formation of a 6-coordinate heme−NO complex. The presence of a second NO molecule in the aa_3 active site strongly modifies the heme−NO EPR spectrum and can be rationalized by a rotation of the Fe−N−O plane with respect to the histidine that coordinates the heme iron. This proposal is supported by molecular-modeling studies that indicate a ∼63° rotation of heme-bound NO upon binding of a second NO to the close-lying copper center CuB. It is argued that the second NO binds to CuB.

The signaling molecule nitric oxide (NO) is involved in the regulation of numerous biochemical processes, including cellular respiration (*1*−*3*). This regulation of respiration takes place by interactions between NO and cytochrome *c* oxidase (C*c*O).[1] One way in which this occurs is via competitive binding of NO at the oxygen binding and reduction site of fully reduced cytochrome oxidase (*1*, *4*).

The C*c*O active site comprises two cofactors, heme a_3 and a nearby copper atom, CuB. Both are able to bind external ligands; the substrate O_2 of the enzyme presumably intermediately binds to reduced CuB on its way to heme a_3 (*5*), where it remains bound during the four-electron reduction reaction. Other diatomic inhibitor ligands such as cyanide (CN), carbon monoxide (CO), and NO can also bind to heme a_3. For CO, a doorstep role of CuB has been established, where CO resides for microseconds during transfer both in to and out of the active site (*6*). For NO, such a role for CuB is less certain and at least any intermediately formed CuB^+−NO is much shorter lived, as inferred from the binding kinetics to heme a_3, which do not appear to saturate with the NO concentration, and from the nanosecond geminate recombination observed after dissociation of NO (*5*). On the other hand, it is possible that two NO molecules are accommodated by the active site (*1*). This has been reported in steady-state electron paramagnetic resonance (EPR) (*7*) and Fourier transform infrared (FTIR) studies (*8*) under high NO concentrations; by contrast, NO uptake experiments at low concentrations indicate stoichiometric uptake of NO on the time scale of ∼1 min (*9*, *10*). Generally, the (temporal) copresence of two NO molecules in the reduced active site is required for any NO reductase activity ($2NO + 2e^- + 2H^+ \rightarrow N_2O + H_2O$). Such an activity has been observed in a number of heme−copper oxidases, in degrees varying from as much as ∼1% of that of heme−iron NO reductases in terminal oxidases from *Thermus thermophilus* (*10*) to virtually 0% in mitochondrial cytochrome *c* oxidase (*7*, *11*).

[†] This work was supported by the CNRS program "Physique et Chimie du Vivant".

* To whom correspondence should be addressed. Phone: +33-1-69334777. Fax: +33-3-69333017. E-mail: marten.vos@polytechnique.fr.

[‡] Ecole Polytechnique-ENSTA.

[§] Institut de Biologie Structurale et Microbiologie.

[||] Institut de Biologie Physico-Chimique.

[⊥] Paul Scherrer Institute.

[1] Abbreviations: C*c*O, cytochrome *c* oxidase; EPR, electron paramagnetic resonance; FTIR, Fourier transform infrared.

10.1021/bi0488808 CCC: $27.50
Published on Web 10/16/2004

NO can be photodissociated from reduced hemes in heme proteins with near unity quantum yield (*12*). Using this property, we have reported a pronounced effect of the NO/enzyme stoichiometry on the picosecond NO-rebinding kinetics after dissociation from reduced C*c*O aa_3 from *Paracoccus denitrificans* (*13*), an effect which we ascribed to the presence of two NO molecules in the active site at higher NO concentrations. One NO molecule binds to heme a_3, but the second NO binding site was not clearly identified. Also the limited time span of these dynamics prohibited until now to discriminate between models of NO−NO interaction during dissociation. With the aim to resolve these issues and to gain insight in the factors determining the reactive behavior of reduced oxidases with NO, we undertook the present study of the NO-rebinding kinetics in this bacterial enzyme, extended from picoseconds to the nanosecond and millisecond time scales, as well as an EPR characterization of the initial states under various NO/enzyme stoichiometries. A comparison is made with C*c*O ba_3 from *T. thermophilus* (*14*), where substantial NO-reductase (*10*) activity precludes the long-lived presence of two NO molecules.

MATERIALS AND METHODS

C*c*O aa_3 from wild-type *P. denitrificans* was purified as described (*15*) from cells grown at low manganese concentrations (*16*). C*c*O ba_3 from *T. thermophilus* was purified as described by Soulimane et al. (*17*).

The enzyme concentrations used were ∼15 and ∼35 μM for the nanosecond and femtosecond optical experiments, respectively, and ∼50 μM for the EPR experiments. The samples were extensively degassed in a gastight vial using a home-built stainless steel gas train and reduced using 10 mM sodium ascorbate and 10 μM (aa_3 from *P. denitrificans*) or 100 μM (ba_3 from *T. thermophilus*) ruthenium hexamine. The samples (80−150 μL for the optical experiments and 250 μL for the EPR experiments) were transferred into a degassed gastight optical cell (Hellma, 117.007 QS, optical path length of 1 mm) or EPR tube, sealed with a rubber septum. The indicated stoichiometries refer to the ratios of absolute amounts of NO and enzyme (in nanomoles) present in the sample cell. Additions of defined volumes of 1% NO gas (in argon) were performed using airtight microliter syringes. The samples were equilibrated for 10 min at room temperature prior to measurements. Using this method, because of equilibration between the headspace and the liquid phase of the cell, for C*c*O aa_3, only partial NO binding occurs for low NO/protein stoichiometries (*13*). For relatively low protein concentrations, as used in the experiments with the nanosecond spectrometer (see below), higher NO/protein stoichiometries were needed to obtain complete binding. Therefore, the absolute stoichiometries used in different experimental conditions cannot be directly compared. For C*c*O ba_3, these effects are not observed (see the Results).

Steady-state absorption spectra were recorded using a Shimadzu 1601 UV−vis spectrophotometer.

Femtosecond spectroscopy using 55-fs pump pulses centered at 590 nm and white-light continuum probe pulses was performed as described elsewhere (*12*, *13*). Previous measurements were limited to ∼300 ps. In the present experiments, an additional 1-m delay line was implemented and delays up to several nanoseconds could be recorded.

Absorption changes on the time scale beyond 5 ns were recorded using a home-built nanosecond spectrophotometer described in ref *18*. The exciting flash was provided by a dye laser [595 nm, 5-ns full width at half-maximum (fwhm)] pumped by the second harmonic of a Nd/Yag laser. The absorption changes were probed at discrete wavelengths and delay times after the exciting flash by flashes provided by an optical parametric oscillator pumped by the third harmonic of a Nd/Yag laser (5-ns fwhm). All optical experiments were performed at room temperature.

EPR spectra were taken on a Bruker ElexSys X-band spectrometer fitted with an Oxford Instrument liquid helium cryostat and temperature control system. The redox and ligation state of the sample in the EPR tube was monitored spectrophotometrically immediately before freezing by placing the tube at the entrance slit of a Spectralon integrating sphere connected to a Kontron Uvikon 922 UV−vis spectrophotometer. The $g = 4$ spectral species was quantified by comparison to the spectrum induced by nitrosylating 2-halobenzoate 1,2-dioxygenase from *Pseudomonas cepacia* (*19*).

Molecular modeling of the NO-bound structures of the active site of C*c*O aa_3 from *P. denitrificans* was performed starting from previously generated energy-minimized structures (*13*). To avoid trapping of these structures in local minima, molecular dynamics simulations with an integration time of 1 fs were performed on these structures and the temperature was raised to 300 K in steps of 10 K, with an equilibration time of 1 ps at each temperature. After at least 30 ps of equilibration at 300 K, the temperature was decreased to 20 K in a similar way, and finally, the model structures were obtained by energy minimization. Minimized structures generated in this way after different equilibration times at 300 K (and thus from different room temperature structures) were virtually identical. The molecular dynamics and energy minimizations were performed using version 27 of CHARMM (*20*).

RESULTS

Steady-State Spectra. The steady-state spectra of fully reduced and NO-ligated forms of aa_3 and ba_3 are shown in Figure 1. The aa_3 spectra are similar to those previously described; (*13*) binding of NO to heme a_3 leads to a blue shift of the a_3 absorption bands, for the Soret band clearly out of the ∼444-nm region, where it strongly overlaps with the *a* absorption band. The shape of the NO-binding-induced difference spectrum was independent of the amount of NO added.

For ba_3, the fully reduced spectrum shows well-separated Soret bands from hemes *b* (427 nm) and a_3 (444 nm), as reported previously (*21*, *22*). The NO-ligated spectrum shows a single Soret peak at 427 nm. In the Q region, the *b* band at 558 nm does not change and the a_3 band shifts from ∼612 to 600 nm. The NO-bound *minus* unligated difference spectrum is similar for both enzymes.

Although they contain the same cofactors (heme a_3 and CuB), the interaction and reactivity of the active-site constituents have markedly distinct features in the ba_3 oxidase from *T. thermophilus* as compared to mammalian and bacterial aa_3 oxidases (*23*). In particular, binding of CO to this enzyme leads to formation of only 70% of the heme

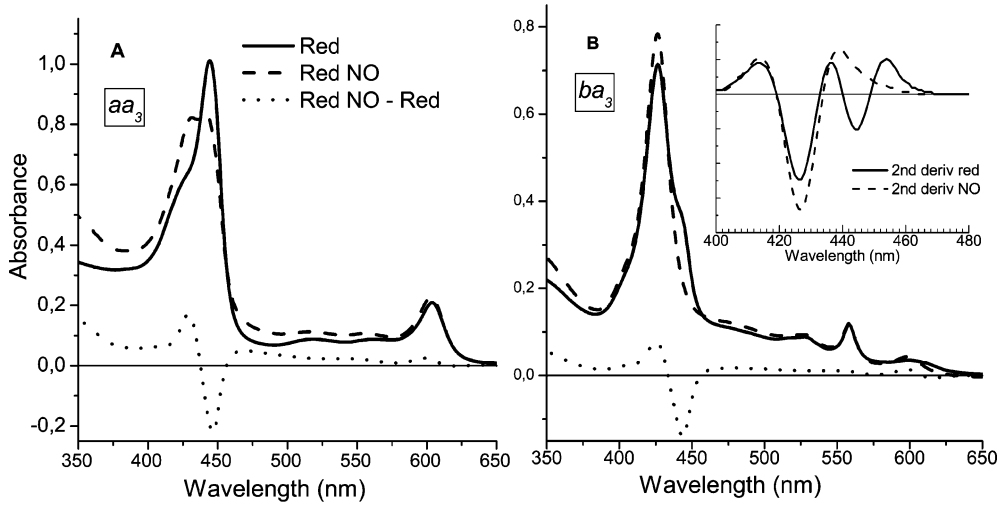

FIGURE 1: Steady-state spectra of fully reduced C*c*O in the unligated state (—) and after equilibration with excess NO (- - -). The dotted lines represent the difference between NO ligated and unligated. (A) C*c*O aa_3 from *P. denitrificans* at 45 μM. (B) C*c*O ba_3 from *T. thermophilus* at 30 μM. (Inset) Second derivative of the Soret region of the absorption spectra of C*c*O ba_3.

a_3−CO complex (*21*, *24*), with the remaining 30% forming a CuB−CO complex (*25*). To estimate the extent of NO binding to heme a_3, the inset of Figure 1B shows the second derivative of the Soret spectra of the unligated and NO-bound forms. In the spectrum of the unligated form, the a_3 shoulder at 444 nm in the absorption band gives rise to a marked second derivative feature. This feature is not observed in the NO-bound form, and, by analysis in comparison with the CO second-derivative spectra (*21*), we estimate that NO-binding occurs for more than 97%. This finding is consistent with the observation that NO complements ligand binding to heme a_3 in the fraction of CO-equilibrated enzymes that does not form the heme a_3−CO complex (*24*).

We observed that upon addition of stoichiometric amounts of NO to reduced ba_3 the a_3−NO complex is rapidly and stably formed for virtually 100%. This behavior, which contrasts with that of the aa_3 enzyme (see the Materials and Methods and ref *13*), is consistent with the proposed high affinity for NO of heme a_3 in C*c*O ba_3 (*10*). It also implies that under these conditions NO is not consumed by NO-reductase activity of the enzyme and that all active sites accommodate 1 NO molecule.

*Picosecond NO Rebinding to C*c*O aa_3 from P. denitrificans.* Previous transient absorption experiments on geminate rebinding of NO with C*c*O demonstrated a ~200−300-ps decay component, which was more pronounced at higher NO concentrations (*13*). These experiments were performed with a time window up to 300 ps (corresponding to a variation of 9 cm in the path length between the pump and probe pulse). Therefore, they did not allow accurate determination of the asymptote of the kinetics and discrimination between an effect of NO concentration on the time constant and on the amplitude of this decay phase. We have now performed such experiments with an extended delay line and a time window up to 2 ns (Figure 2A). The shape of the transient spectra between ~30 ps and 2 ns does not change and corresponds to the steady-state unligated *minus* NO-ligated spectrum. The shape of the transient spectra is also independent of the NO/enzyme stoichiometry (Figure 2B). The amplitude of the transient spectra decays on the subnanosecond time scale and remains constant beyond 1 ns. The kinetics at all NO/enzyme stoichiometries can be fitted with

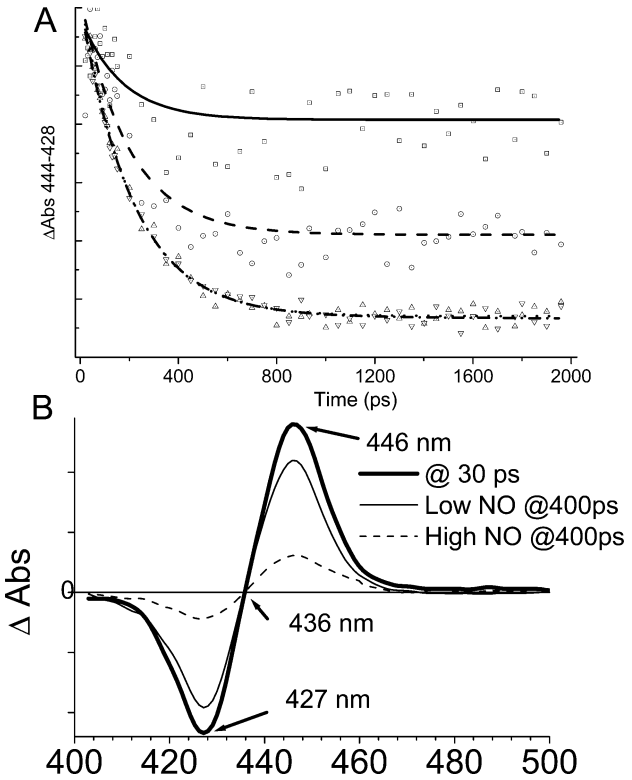

FIGURE 2: (A) Normalized kinetics of geminate recombination of NO and heme a_3 after photodissociation as a function of the NO/C*c*O ratio in C*c*O aa_3 from *P. denitrificans*. Open squares stand for the NO/C*c*O ratio of 1:1; open circles, for 3:1; up triangles, for 10:1; and down triangles, for 130:1. The lines are fits to a 200-ps monoexponential decay and an asymptotic value. (B) Transient spectra of aa_3−NO at t = 30 and 400 ps for NO/C*c*O ratios of 130:1 (···) and 1:1 (—). The traces are normalized at t = 30 ps.

an exponential decay with the same time constant of 200 ps and an asymptotic term. The relative amplitude of the decay component depends on the NO concentration and varies from less than 30% for a NO/protein stoichiometry of 1:1 to 90% for 10:1 or more. Thus, we conclude that the NO concentration influences the relative amplitude rather than the time constant of the decay phase. This indicates that a higher NO/enzyme ratio does not speed up NO recombination (by direct competition between the dissociated NO molecule and

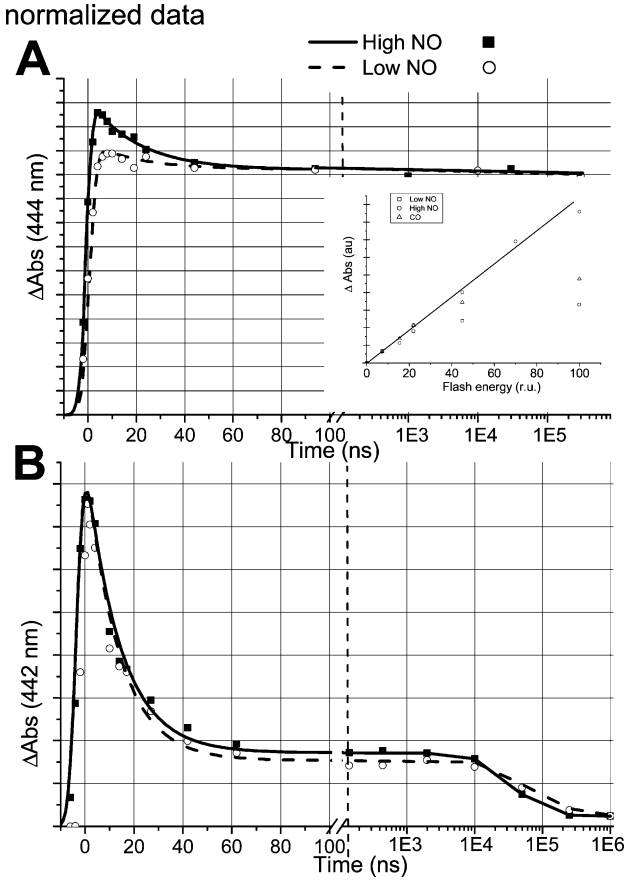

FIGURE 3: Normalized nano- to microsecond kinetics of recombination of NO to heme a_3 after photodissociation as a function of the NO concentration in C*c*O from *P. denitrificans* (A) and *T. thermophilus* (B). The lines are fits as described in the text. From 0 to 100 ns, the scale is linear; beyond 100 ns, it is logarithmic. (■) High (100:1) and (○) low (5:1) NO/enzyme ratio. (Inset) Saturation curve of the intensity of the signal 6 ns after the pulse as a function of the flash energy for C*c*O aa_3 from *P. denitrificans*, normalized in the low-energy region. The dotted line is a guide for the eye.

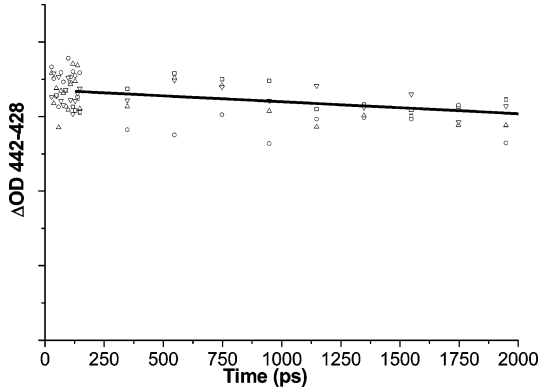

FIGURE 4: Kinetics of geminate recombination of NO and heme a_3 after photodissociation as a function of the NO/C*c*O ratio in C*c*O ba_3 from *T. thermophilus*. Open squares stand for NO/C*c*O ratio of 1:1; open circles, for 3:1; up triangles, for 10:1; and down triangles, for 130:1. The line corresponds to an exponential decay with a time constant of 15 ns (80%) and an asymptotic value (20%), cf. Figure 3B.

another NO molecule present in the heme pocket) but merely favors picosecond rebinding over longer (>2 ns) rebinding processes. The small 200-ps phase at stoichiometric NO concentrations may reflect a fraction of the enzyme accommodating 2 NO molecules (see the EPR characterization below).

Nanosecond−Millisecond NO Rebinding to CcO aa3 from P. denitrificans. Figure 3A displays the recombination kinetics of NO with heme a_3 in C*c*O aa_3 from *P. denitrificans* at longer time scales under low and high NO/enzyme stoichiometry. At high NO concentrations, significant decay phases are observed in the nanosecond time range. A fit to the data yields a decay component with a time constant of 20 ns (amplitude ∼ 25% of the long-lived component for high NO concentrations) and a faster component, which cannot be resolved with the 5-ns time resolution. The latter component presumably reflects the 200-ps phase observed in the femtosecond experiments, but its apparent amplitude is very low in the nanosecond experiment, because the time resolution is much longer than the 200-ps time constant.

The unresolved and 20-ns phases are strongly suppressed at low NO concentrations. For the unresolved phase, this is consistent with the presence of the 200-ps phase being correlated with the high NO concentration (Figure 2A). The result that the 20-ns phase also depends on the NO concentration suggests that it is due to the same rebinding process as the 200-ps phase and that this process is thus multiphasic. Virtually no further decay is observed until the millisecond time scale, where the NO concentration-dependent decay occurs, on a time scale roughly consistent with the reported bimolecular binding constant for the mammalian enzyme (*5*).

The presence of a recombination phase faster than the duration of the 5-ns pump pulse suggests that, within one pulse, recombined heme a_3−NO pairs can be redissociated several times. This feature is indeed observed in the dependence of the net NO dissociation yield on the intensity of the pump pulse (inset of Figure 3A). At low NO concentrations, when the fast phase is relatively weak, the signal saturates at a much lower pulse energy than at high NO concentrations, where absorption of multiple photons can lead to increased net photodissociation on the nanosecond time scale. Fully consistent with this interpretation, the saturation curve at low NO concentration is similar to that of CO dissociation (inset of Figure 3A), where also no geminate recombination occurs (*26*).

NO Rebinding to CcO ba3 from T. thermophilus. Figure 4 shows transient absorption kinetics upon NO dissociation from C*c*O ba_3 on the picosecond and early nanosecond time scale. After ∼30 ps, when all signals related to heme excited states have decayed, the shape of the transient spectra is very similar to those observed for aa_3 and reflects NO dissociation from heme a_3 (not shown). The signals decay only very little (∼10%) on the time scale up to 2 ns, and the decay does not depend on the NO concentration. In particular, we emphasize that no subnanosecond NO-rebinding phase is observed, as it is the case in the aa_3 enzyme.

Extension of these experiments to longer time scales using nanosecond excitation pulses (Figure 3B) shows that the signal decays for ∼80% with a time constant of ∼15 ns, in quantitative agreement with the weak decay observed in the ultrafast experiments above. The remaining signal decays in the ∼50 μs time range, depending slightly on the NO concentration, and substantially faster than the bimolecular rebinding observed in the aa_3 enzyme. The NO consumption

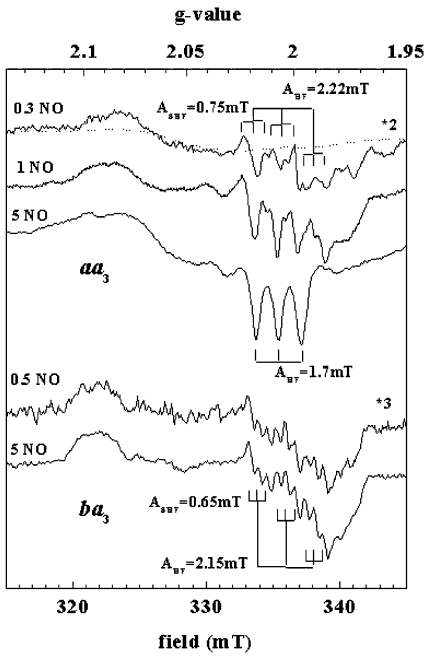

FIGURE 5: EPR spectra recorded on reduced C*c*O aa_3 from *P. denitrificans* (upper) and C*c*O ba_3 from *T. thermophilus* (lower) at various NO/enzyme stoichiometries as indicated for each spectrum. The dotted line superimposed on the upper spectrum corresponds to unligated aa_3. Instrument settings: temperature, 50 K; microwave frequency, 9.42 GHz; microwave power, 6.7 mW; and modulation amplitude, 0.1 mT.

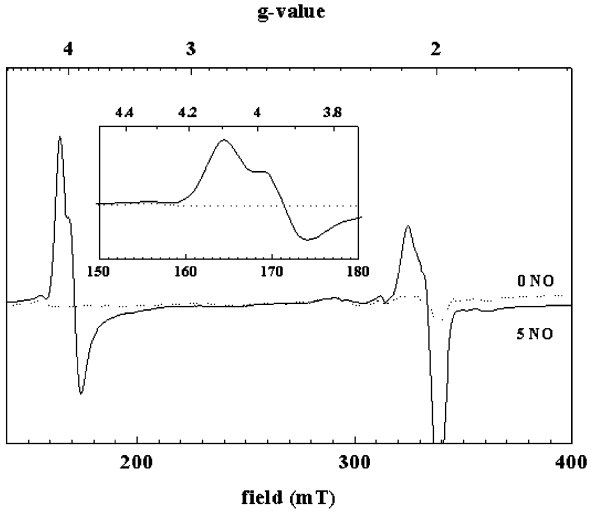

FIGURE 6: EPR spectra recorded on reduced nitrosylated C*c*O aa_3 from *P. denitrificans* in the absence (···) and presence (—) of excess NO. (Inset) Expanded spectrum in the $g = 4$ region. Instrument settings: temperature, 15 K; microwave frequency, 9.42 GHz; microwave power, 6.7 mW; and modulation amplitude, 2.8 mT.

precludes the reliable determination of a second-order binding constant in this way, but we note that the NO concentration in solution must be far less than 10 μM for all concentrations studied. Assuming that this phase reflects bimolecular binding, we find a lower limit for the second-order NO association constant of 20×10^9 M^{-1} s^{-1}, much higher than the value of 105×10^6 M^{-1} s^{-1} reported for the mammalian aa_3 enzyme (*5*). An alternative interpretation of this phase is that it reflects heme a_3—NO geminate recombination with NO accommodated at a different site as CuB. Indeed, for photodissociated CO, such a site has recently been proposed on the basis of time-resolved FTIR experiments (*27*).

EPR Characterization. In an effort to characterize the steady state of the various NO-bound states of the active sites of aa_3 and ba_3 oxidases, EPR spectra were recorded on samples frozen from similar conditions as the flash photolysis experiments. Substoichiometric NO/enzyme ratios induced the appearance of roughly similar EPR spectral features in the $g = 2$ region in both, the aa_3 and the ba_3 oxidases (Figure 5). The respective spectra are characteristic of nitric oxide bound to heme at the 6th coordination position with an imidazole ligand occupying the 5th position. Corresponding EPR spectra have been recorded on nitrosylmyoglobin and hemoglobin (*28*—*31*), as well as on nitrosylated porphyrin model compounds (*32*). Isotope exchange experiments and single-crystal EPR studies in these systems have allowed to attribute the dominant 3-line hyperfine structure at the intermediate *g* value (around $g = 2$) to the interaction of the unpaired electron with the nuclear spin ($I = 1$) of the NO—nitrogen nucleus (*30*, *32*). For the case of the aa_3 and ba_3 oxidases studied in this work, hyperfine coupling constants (A_{HF}) of 2.22 and 2.15 mT, respectively, are observed (Figure 5). The additional superhyperfine structure was previously shown to arise from the interaction of the electron spin with the ($I = 1$) nucleus of the Fe-ligating nitrogen on the imidazole serving as the 5th ligand (*30*, *32*). The A_{SHF} constants for this interaction were determined at 0.75 and 0.65 mT for the aa_3 and the ba_3 oxidases, respectively. Corresponding spectra have previously been obtained for NO bound to the mitochondrial cytochrome oxidase aa_3 (*33*—*35*). The spectra shown in Figure 5 were recorded at 50 K. At lower temperatures, the signal intensity increases but the hyperfine structure becomes substantially less well-resolved.

Whereas for substoichiometric amounts of NO, C*c*O aa_3 and ba_3 behaved similarly, increasing the NO levels to stoichiometric and suprastoichiometric amounts induced strongly divergent EPR spectra in both enzymes. While, in C*c*O ba_3, the spectrum only increased in intensity without modification of spectral features, the EPR spectrum of nitrosylated aa_3 oxidase from *P. denitrificans* changed drastically. At 5 NO/enzyme, the hyperfine interaction with the NO nitrogen has decreased to $A_{HF} = 1.6$ mT and the superhyperfine structure has completely disappeared. At stoichiometric amounts of NO/enzyme, a mixed spectrum is observed containing features of both, the low-NO and the high-NO spectral species. The loss of lines in the region above 338 mT upon increasing NO to suprastoichiometric levels demonstrates that the high-NO spectrum results from a transformation of the low-NO species rather than to a superposition of two different spectral forms. This conclusion is corroborated by the observation that the double integral of the spectra remains constant within experimental accuracy above an NO/enzyme ratio of about 1 (data not shown). As will be explained in the Discussion, we propose that the transformation of the spectrum corresponds to a rotation of the Fe—N—O plane with respect to the plane of the histidine coordinating the heme iron.

Spectra taken at 15 K on the aa_3 oxidase show the appearance of a new paramagnetic species for NO/enzyme ratios above 1 (Figure 6). This paramagnetic center is characterized by a peak-shaped feature at $g = 4.1$ directly

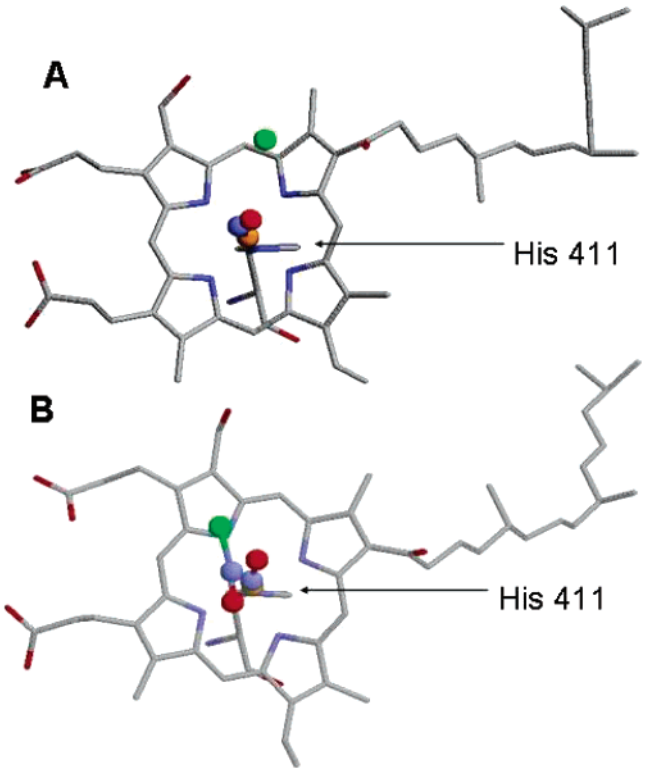

FIGURE 7: Modeled structures of the active site of C*c*O aa_3 from *P. denitrificans* with NO bound to heme a_3 (A) and on both heme a_3 and CuB (B). Cu_B is colored in green, and Fe−a_3 is colored in gold. The plane of His 411 is perpendicular to the plane of representation. The figure was prepared using RASMOL (*59*).

followed by a derivative line at $g = 3.95$. No hyperfine structure is observed on these lines (see the inset of Figure 6).

In stark contrast to these observations on the aa_3 enzyme, only a single paramagnetic species, i.e., that shown in the bottom of Figure 5, was observed in the ba_3 oxidase at all NO/enzyme ratios examined.

Molecular Modeling. The EPR studies indicate changes in the orientation of the heme-bound NO with respect to the plane of the histidine (His 411) in the presence of a second NO, at least at cryogenic temperatures. Inspection of the model energy-minimized structures generated previously with NO bound to heme a_3 only and to both heme a_3 and CuB (*13*) appeared in qualitative agreement with this observation. To further validate these models and to avoid trapping in local minima, we have now generated minimized models after warming the structures to 300 K and recooling. Figure 7 shows relevant features of them. As reported in our previous modeling (*13*), the models show substantial motion of CuB upon its binding to NO, with weakening of the CuB−His 276 interaction. In addition, the present representation makes clear that the heme-bound NO rotates substantially; the Fe−N−O plane is nearly parallel to that of His 411 (14°) in the 1-NO model but nearly perpendicular (77°) in the 2-NO model.

DISCUSSION

We have carried out a comprehensive study of the binding and dynamics of NO in the active site of the bacterial heme−copper oxidases aa_3 and ba_3. The earlier observed effects of NO/enzyme stoichiometry on the picosecond heme−NO-rebinding kinetics in aa_3 (*13*) were now extended to and also observed on longer time scales. Along with the novel EPR characterization and the comparison with ba_3, they further confirm the assessment that two NO molecules can be accommodated by the active site at relatively low NO concentrations and allow proposing structural characteristics of the NO accommodation.

Kinetics of Heme a_3−NO Rebinding. Previously, we had observed that the kinetics of NO rebinding to heme a_3 in C*c*O aa_3 from *P. denitrificans* on the time scale up to 300 ps are NO concentration-dependent (*13*). Our present results on a far more extended time scale (Figure 2A) demonstrate that the kinetics on the subnanosecond time scale can be described by a single 200-ps decay phase and a virtually nondecaying phase, with the relative amplitude of the 200-ps phase increasing with an increasing NO concentration. They discard the alternative possibility of a NO concentration-dependent time constant as expected for competition for heme binding between the dissociated NO molecule and other (intraprotein) NO molecules. Thus, we can now attribute this phase to recombination of heme a_3 to one single NO molecule, with this recombination being induced by the presence of a second NO molecule in/near the heme pocket, an attribution favored but not proven previously (*13*). The interpretation of the kinetics in terms of geminate rebinding taking place or not on the subnanosecond time scale is further strengthened by the NO concentration dependence of the saturation curve of NO dissociation on the nanosecond time scale (inset of Figure 3A).

In addition, another, 20-ns, NO concentration-dependent phase was detected (amplitude ∼ 2% of the total decay for high NO concentrations). Multiphasic geminate rebinding of NO with heme in proteins is commonly observed (*12*, *36*, *37*) and is thought to reflect at least in part relaxation processes of the protein, leading to increasingly high rebinding barriers as a function of time. For the case of the aa_3−NO complex at high NO concentrations, the time scale of these phases are well-separated (a dominant 200-ps phase followed by a minor 20-ns phase), suggesting clearly distinct recombination mechanisms. The 20-ns phase presumably reflects rebinding with NO from outside the active site, in competition with NO diffusion out of the protein. Our nanosecond results are in general agreement with those of Blackmore and co-workers (*5*), who monitored NO recombination with the mammalian aa_3 enzyme using 532 nm, 9-ns flashes, and under conditions of high NO concentrations (0.1 atm) and found two decay phases in the 10−100-ns range.

At low NO concentration, virtually no geminate rebinding takes place. Assuming NO intermediately binds to CuB and taking into account the lower limit of ∼10 μs for the time constant of NO transfer from CuB to heme a_3 (*5*), this indicates that NO dissociates from CuB on the nanosecond time scale and diffuses out of the protein. This finding implies that under these conditions, once dissociated from heme a_3, virtually all NO molecules leave the protein, as is the case with CO as a ligand. This property, in itself very unusual for NO rebinding in heme proteins, possibly indicates a role of CuB as a gateway for ligand shuttling, even for NO.

Comparison ba_3 and aa_3. An important general result is that, in contrast to the aa_3 enzyme, NO concentration dependence was not observed in the ba_3 enzyme, neither in

the NO-rebinding dynamics nor in the steady-state EPR characterization. For all NO concentrations, the picosecond recombination kinetics (virtually no rebinding) and the EPR characterization are similar to the aa_3 low NO concentration case. Because this enzyme has a considerable NO-reductase activity (two NO molecules are reduced to N_2O and H_2O), the *steady-state* copresence of two NO molecules in the active site is virtually precluded. Thus, this result strongly supports the idea of multiple NO molecules in/near the active site of aa_3.

In ba_3, a major NO−heme a_3 recombination phase with a time constant of ~15 ns is observed. Assuming dissociated NO intermediately binds to CuB, this phase reflects the competition between the transfer back to heme a_3 (80%) and diffusion to another docking site (*27*) or out of the protein (20%). The much higher yield of recombination compared to the aa_3 low NO concentration case indicates a high NO affinity of heme a_3 in ba_3, possibly because the channel out of the protein from CuB is more blocked, as appears to be the case for CO (*27*). An intriguing and possibly related observation is that, despite the well-documented NO-reductase activity (*10*), the ba_3−NO complex was readily formed and very stable upon stoichiometric addition of NO to the complex. This must indicate that the affinity of the active site for a single NO is high compared to the affinity for a second NO (which would lead to N_2O formation and loss of the ba_3−NO complex) in this enzyme. A quite different behavior occurs in the aa_3 enzyme: at NO addition in the stoichiometric range, the aa_3−NO complex is only partially formed and the second site (presumably CuB) is filled at relatively low NO concentrations. One might speculate that this behavior is also related to the higher affinity of ba_3 oxidase for oxygen as compared to aa_3 from *P. denitrificans* (*23*).

Interpretation of Spectral Species in the g = 2 Region. As already detailed in the Results, the EPR spectra obtained on the aa_3 oxidase in the presence of low NO/enzyme stoichiometries and on the ba_3 enzyme both at low- and high-NO levels are readily interpreted as resulting from NO bound to heme a_3, the second axial ligand of which is a histidine. The spectrum observed in the presence of suprastoichiometric amounts of NO strongly resembles those reported for nitrosyl heme with a ruptured Fe−His bond. Corresponding spectral changes have been observed in nitrosyl hemoglobins upon transition between the R and the T state and are interpreted to reflect the movement of the iron atom into the heme plane in the hemoglobin α chains, entailing breakage of the bond toward the histidine.

A spectrum similar to that shown in Figure 5 for high levels of NO has recently been published for the mitochondrial enzyme (*38*) and was interpreted in the framework of the hemoglobin literature and by comparison to extracted, nitrosylated heme *a* as demonstrating the presence of pentacoordinated heme a_3. For the case of our experiments, this interpretation of the high-NO spectral species would mean that the presence of more than one NO molecule in the catalytic pocket either pulls the Fe−NO moiety toward CuB or pushes the axial histidine away from heme a_3. Such conformational changes appear highly unlikely to us given the available structural information as detailed in the following.

"Hexacoordinated" EPR spectra are observed in nitrosyl hemoglobin β chains and nitrosyl myoglobin, showing Fe−His bond lengths of 2.1−2.3 Å, respectively (e.g., see PDB entries 1RPS, 1NPF, or 1HJT). These values are almost identical to those observed in deoxyhemoglobin and myoglobin (about 2.2 Å) (1RQ3). The iron in the pentacoordinated heme of α chains in the R state of NO−Hb, however, is at a distance of 4.1 Å from the proximal histidine (1RPS). The corresponding Fe(a_3)−His bond length in the deoxy state of aa_3 oxidase is 2.1 and 1.9 Å for the *P. denitrificans* and the bovine enzymes, respectively, i.e., very similar to those in hexacoordinated hemoglobin and myoglobin. Unfortunately, no X-ray structural data are available for oxidases with nitric oxide ligands. Nonetheless, the 3D structures of the mitochondrial aa_3 oxidase seem to show that, while CuB moves significantly in response to changes in the redox and ligation states of the enzyme (as also observed in our modeling of the bacterial enzyme), the position of the iron in heme a_3 as well as that of the histidine are roughly identical in the different states examined (i.e., oxidized, reduced, and in the presence of carbon monoxide and azide) (*39*). This argues against the existence of a variable Fe−His distance as it is found in the hemoglobins and thus makes the observation of the "pentacoordinated" spectrum difficult to rationalize. Despite the crystallographic evidence, Pearce et al. (*38*) have proposed far-going structural flexibility of the histidine−heme a_3 bond based on the observation that the respective bond length is 3.3 Å in the *T. thermophilus* ba_3 oxidase, i.e., significantly larger than what is observed for the two aa_3 oxidases and about halfway between the values of pentacoordinated (4.1 Å) and hexacoordinated (2.2 Å) hemoglobins. However, it is precisely in the ba_3 oxidase with its unusually long bond where a "hexacoordinated" spectrum is observed for all NO levels (bottom of Figure 5).

In summary, the sets of Fe−His bond lengths and the various types of EPR spectra do not yield a consistent picture. We therefore favor a different physical rationalization of the observed spectra. As can be seen from the spectra containing the superhyperfine interaction (Figure 5), the g tensor is rhombic with $g_{max} = 2.1$, $g_{int} = 2$, and $g_{min} = 1.98$. This rhombicity implies that the unpaired electron must reside to a significant level in a molecular π orbital involving the p orbital of the sp^2-hybridized nitrogen of the NO moiety and the d_{xz} (or d_{yz}) orbital of the iron, in addition to the σ-type molecular orbital formed by the iron d_{z^2} and a nitrogen sp^2 orbital. EPR studies on single crystals of MbNO have demonstrated the validity of this bonding scheme (*30*). In all X-ray structures of MbNO and HbNO in states where the "hexacoordinated" spectrum is observed, the Fe−N−O plane lies roughly (within 15°) parallel to the plane of the proximal histidine. This implies that the π-molecular orbital mentioned above will extend to the p orbital of the 5th ligand nitrogen of the histidine, rationalizing the comparatively strong (considering the distance between the nitric oxide ligand and the histidine) A_{SHF} value of about 0.7 mT. In this context, it is noteworthy that single-crystal EPR results suggest the superhyperfine coupling to be strongly anisotropic (*30*, *40*), excluding the possibility that it arises merely from Fermi contact interaction through the σ-bonding orbitals of the NO−Fe−His system.

Correspondingly, in β chains of HbNO in the state where the bond to the axial histidine is cleaved (*41*) and where a "pentacoordinated" EPR spectrum is observed, the NO ligand is substantially turned away from the histidine plane projection onto the heme plane (by >25°).

Considering these results, we propose that in the aa_3 oxidase the transition from the low- to high-NO spectral species reflects a rotational movement of the NO ligand with respect to the heme normal rather than the absence of the 5th ligand as observed in model systems. At low NO levels, the EPR results thus predict a binding geometry of NO to heme a_3 placing the Fe−N−O plane roughly coplanar with the histidine ligand plane. At high NO concentrations, the nitrosyl ligand would be turned away from this conformation by at least 20°, thus precluding the formation of the π orbital extending from the nitric oxide through to the histidine ligand. The molecular-modeling studies (Figure 7) indeed predict such rotational movements, by assuming that a second NO binds to CuB.

Origin of the Signal in the g = 4 Region Observed in aa_3 at High NO/Enzyme Stoichiometry. In contrast to the spectral species detected in the $g = 2$ region, the signal at about $g = 4$ does not resemble spectra previously reported for heme or copper compounds and its interpretation is therefore far from trivial. Spectra reminiscent of that shown in Figure 6 have been detected in nitrosylated copper pairs (*42*−*46*) or in NO-treated cytochrome oxidase in the presence of azide (*35*, *47*, *48*). In all of these cases, the $g = 4$ signals have been interpreted (*49*) as arising from the $\Delta m_S = 2$ transition within a triplet state formed by the spin on NO bound to ferrous heme (in the case of cytochrome oxidase) or to Cu^I and the spin on a Cu^{II} ion (either oxidized CuB or the second copper in the Cu pairs). In all of these mentioned cases, hyperfine lines because of interaction with the $I = 1$ copper nucleus/nuclei are observed. No such hyperfine lines are present in the spectrum shown in the inset of Figure 6, and therefore, this appears an unlikely interpretation of our results. We furthermore did not see any measurable amounts of Cu^{II} in the optical spectra recorded prior to freezing the samples. Alternatively, the spectrum might arise from the $\Delta m_S = 2$ transition within a triplet state formed by two NO ligands, one bound to heme a_3 and the other bound to CuB. This would explain the absence of a copper hyperfine structure and would be in line with the presence of reduced copper. However, if this interpretation was correct, the appearance of the triplet signal should go hand in hand with the loss of the heme a_3−NO spectrum. This is not observed, and therefore, we also consider this model as unlikely.

Intriguingly, the spectrum shown in Figure 6 is practically identical to spectra reported for nitric oxide bound to mononuclear non-heme iron centers such as, for example, in nitrosylated bacterial dioxygenases (*50*, *51*). The paramagnetic species giving rise to this spectrum has been identified as an $S = {}^3/_2$ spin state formed in the $\{Fe{-}NO\}^7$ electronic system. NO is considered to formally oxidize Fe^{II} to Fe^{III} resulting in an $S = 1$ state on the NO ligand. The $S = 1$ spin couples antiferromagnetically to the high spin $S = {}^5/_2$ state of Fe^{III}, yielding a resulting spin of ${}^3/_2$ for the whole spin system (*51*). Quantification of this spectrum by comparison to that of a nitrosylated bacterial dioxygenase showed that the signal corresponds to 40−70% (20−35 μM) of aa_3 oxidase present in the sample. This renders the possibility that the signal arises from an impurity quite unlikely. In C*c*O, however, no non-heme iron atom appears to be present. The only conceivable metallic binding site for a second nitric oxide is CuB. Considering the electronegativity of these reaction partners, there is indeed a high chance that NO formally oxidizes Cu^I to Cu^{II} in the $\{Cu{-}NO\}^{11}$ electronic system. To produce an $S = {}^3/_2$ spin state, the resulting $S = 1$ on the NO ligand must then couple ferromagnetically (rather than antiferromagnetically as inferred for the iron case mentioned above) with the $S = {}^1/_2$ spin of Cu^{II}. Because the spin on Cu^{II} resides in an almost filled d shell, whereas the d orbitals in Fe^{III} are only half-filled, an inverse sign for the coupling of the two systems is not excluded.

The interpretation of the observed spectrum as an $S = {}^3/_2$ state formed by NO bound to reduced copper explains both, the EPR spectral parameters of this paramagnetic species and the persistence of the heme a_3−NO spectrum upon formation of the $g = 4$ species. We therefore favor this model at the time being.

Unfortunately, suitable copper model systems for comparison are presently not available in the literature. The only well-studied model systems are nitrosylated Cu zeolites. The copper core in these model compounds is in a distorted tetrahedral environment with a C_3 symmetry along the Cu−NO bond (*52*). In cytochrome oxidases, by contrast, the copper and nitrogen atoms of the three-coordinated histidines are almost in plane and the ligand geometry around the copper center is far from being C_3-symmetric. Crystal structures of C*c*O aa_3 enzymes in different conditions (*39*, *53*−*55*) furthermore suggest the possibility of cleavage of the bond between CuB and one of its histidine ligands under certain circumstances, which would imply an even more unconventional ligation pattern at the CuB core. Our modeling of the active site with NO bound to CuB also indicates substantial weakening of the CuB−His 276 interaction upon binding of NO to CuB. In any case, however, the binding conformation of NO−CuB must drastically differ from that observed in the Cu zeolites, rationalizing the absence of paramagnetic species reported for these model compounds (*56*, *57*).

Recently, the 3D structure of the copper−nitrosyl complex in dissimilatory nitrite reductase has been reported (*58*). The ligation geometry of the copper ion by three histidine residues remotely resembles that found in C*c*Os. The NO molecule, however, was found to be bound "side-on" to the Cu atom, i.e., with N and O of the N−O moiety equidistant from Cu. As evidenced by the observation of a Cu^{II} EPR spectrum, the nitroxide abstracted an electron from copper upon binding to this enzyme. This particular system, despite some structural similarities to the Cu site in C*c*O, is thus still not helpful in interpreting our EPR results.

Comparison to Previous EPR Studies. The interactions of NO with heme−copper oxidases, as probed by EPR spectroscopy, are quite complex. The presence of a "hexacoordinated" spectrum at low NO concentrations and an EPR silent state attributed to antiferromagnetic interaction between a_3- and CuB-bound nitric oxides at high NO levels has been reported (*7*, *35*). By contrast, "hexacoordinated" spectra have been observed also at saturating NO levels (*33*−*35*). Recently, Pearce et al. (*38*) have reported the observation of "pentacoordinated" and mixed (hexa- and pentacoordinated) spectra similar to our aa_3 spectra at stoichiometric

and suprastoichiometric amounts as shown in Figure 5.

In principle, the divergent results might be attributed to the use of differing sources for aa_3 oxidase, i.e., *P. denitrificans* in our case and bovine mitochondria in all other mentioned cases. However, the fact that Pearce et al. (*38*) observed similar spectra as ours in the bovine enzyme, albeit for different states of samples, renders this possibility unlikely. We therefore tend to believe that the differing results are actually because of differing states of the sample. In our hands, optical verification of the redox and heme-ligation states of samples *in the EPR tube* prior to freezing proved crucial for obtaining reproducible results. In addition, we note that (a) our results were obtained at very low levels of NO, the saturation effects in aa_3 at ~5 NO/enzyme in the EPR experiments correspond to equilibration with less than 0.001 atm of NO, and (b) reduction by dithionite was avoided.

CONCLUDING REMARKS

The ensemble of our results clearly demonstrate that two NO molecules can be accommodated by the active site of C*c*O aa_3, one bound to heme a_3 and one presumably at CuB. The CuB-bound NO clearly influences the configuration of the NO−heme bond and de facto stabilizes it by favoring its reformation after dissociation into different configurations (i.e., on the picosecond and nanosecond time scale). Both, the EPR results and molecular modeling indicate that the bent Fe−N−O configuration allows steric flexibility and makes it possible to accommodate the 2 ligand molecules in the active site. The Fe−C−O configuration, by contrast, is intrinsically stretched, and this may explain why 2 CO molecules are not accommodated by the active site (*8*, *39*). Along the same line of reasoning and taking into account the bent Fe−O−O configuration, one might speculate that 2 O_2 molecules or, probably more relevantly, O_2 and NO can be copresent in the active site.

Finally, our results yield a consistent picture of the NO-interaction properties of the reduced ba_3 oxidase in comparison with the aa_3 oxidase. Evidence for only one NO steadily and with high affinity bound to the active site was found, in a configuration similar to that for the aa_3 1-NO case, in agreement with the finding that a second NO would lead to NO reduction (*10*). In ba_3, the relative affinity of accommodation of a second NO after formation of the heme a_3−NO bond is substantially lower than in aa_3, a property that may be related to the relatively small Fe a_3−CuB distance (*23*).

ACKNOWLEDGMENT

We thank Jean-Louis Martin for stimulating discussions and Audrius Jasaitis for critical reading of the manuscript.

REFERENCES

1. Cooper, C. E. (2002) Nitric oxide and cytochrome oxidase: Substrate, inhibitor or effector? *Trends Biochem. Sci. 27*, 33−39.
2. Moncada, S., and Erusalimsky, J. D. (2002) Does nitric oxide modulate mitochondrial energy generation and apoptosis? *Nature Rev. Mol. Cell Biol. 3*, 214−220.
3. Brunori, M., Giuffre, A., Forte, E., Mastronicola, D., Barone, M. C., and Sarti, P. (2004) Control of cytochrome *c* oxidase activity by nitric oxide, *Biochim. Biophys. Acta 1655*, 365−371.
4. Giuffre, A., Sarti, P., D'Itri, E., Buse, G., Soulimane, T., and Brunori, M. (1996) On the mechanism of inhibition of cytochrome *c* oxidase by nitric oxide, *J. Biol. Chem. 271*, 33404−33408.
5. Blackmore, R. S., Greenwood, C., and Gibson, Q. H. (1991) Studies of the primary oxygen intermediate in the reaction of fully reduced cytochrome oxidase, *J. Biol. Chem. 266*, 19245−19249.
6. Einarsdottir, O. (1995) Fast reactions of cytochrome oxidase, *Biochim. Biophys. Acta 1229*, 129−147.
7. Brudvig, G. W., Stevens, T. H., and Chan, S. I. (1980) Reactions of nitric oxide with cytochrome *c* oxidase, *Biochemistry 19*, 5275−5285.
8. Zhao, X. J., Sampath, V., and Caughey, W. S. (1994) Infrared characterization of nitric oxide bonding to bovine heart cytochrome *c* oxidase and myoglobin, *Biochem. Biophys. Res. Comm. 204*, 537−543.
9. Stubauer, G., Giuffre, A., Brunori, M., and Sarti, P. (1998) Cytochrome *c* oxidase does not catalyze the anaerobic reduction of NO, *Biochem. Biophys. Res. Comm. 245*, 459−465.
10. Giuffrè, A., Stubauer, G., Sarti, P., Brunori, M., Zumft, W. G., Buse, G., and Soulimane, T. (1999) The heme-copper oxidases of *Thermus thermophilus* catalyze the reduction of nitric oxide: Evolutionary implications, *Proc. Natl. Acad. Sci. U.S.A. 96*, 14718−14723.
11. Sarti, P., Giuffre, A., Barone, M. C., Forte, E., Mastronicola, D., and Brunori, M. (2003) Nitric oxide and cytochrome oxidase: Reaction mechanisms from the enzyme to the cell, *Free Radical Biol. Med. 34*, 509−520.
12. Martin, J.-L., and Vos, M. H. (1994) Femtosecond spectroscopy of ligand rebinding in heme proteins, *Methods Enzymol. 232*, 416−430.
13. Vos, M. H., Lipowski, G., Lambry, J.-C., Martin, J.-L., and Liebl, U. (2001) Dynamics of nitric oxide in the active site of reduced cytochrome *c* oxidase aa_3, *Biochemistry 40*, 7806−7811.
14. Soulimane, T., Buse, G., Bourenkov, G. P., Bartunik, H. D., Huber, R., and Than, M. E. (2000) Structure and mechanism of the aberrant ba_3-cytochrome *c* oxidase from *Thermus thermophilus*, *EMBO J. 19*, 1766−1776.
15. Liebl, U., Lipowski, G., Negrerie, M., Lambry, J.-C., Martin, J.-L., and Vos, M. H. (1999) Coherent reaction dynamics in cytochrome *c* oxidase, *Nature 401*, 181−184.
16. Seelig, A., Ludwig, B., Seelig, J., and Schatz, G. (1981) Copper and manganese electron spin resonance studies of cytochrome *c* oxidase from *Paracoccus denitrificans*, *Biochim. Biophys. Acta 636*, 162−167.
17. Soulimane, T., Gohlke, U., Huber, R., and Buse, G. (1995) Three-dimensional crystals of cytochrome-*c* oxidase from *Thermus thermophilus* diffracting to 3.8 Å resolution, *FEBS Lett. 368*, 132−134.
18. Béal, D., Rappaport, F., and Joliot, P. (1999) A new high-sensitivity 10-ns time-resolution spectrophotometric technique adapted to in vivo analysis of the photosynthetic apparatus, *Rev. Sci. Instrum. 70*, 202−207.
19. Riedel, A., Fetzner, S., Rampp, M., Lingens, F., Liebl, U., Zimmermann, J.-L., and Nitschke, W. (1995) EPR, electron spin-echo envelope modulation, and electron nuclear double resonance studies of the 2Fe2S centers of the 2-halobenzoate 1,2-dioxygenase from *Burkholderia (Pseudomonas) cepacia* 2CBS, *J. Biol. Chem. 270*, 30869−30873.
20. Brooks, B. R., Bruccoleri, R. E., Olafson, B. D., Swaminathan, S., and Karplus, M. (1983) CHARMM: A program for macromolecular energy, minimization, and dynamics calculations, *J. Comput. Chem. 4*, 187−212.
21. Goldbeck, R. A., Einarsdottir, O., Dawes, T. D., O'Connor, D. B., Surerus, K. K., Fee, J. A., and Kliger, D. S. (1992) Magnetic circular dichroism study of cytochrome ba_3 from *Thermus thermophilus*: spectral contributions from cytochromes *b* and a_3 and nanosecond spectroscopy of carbon monoxide photodissociation intermediates, *Biochemistry 31*, 9376−9387.
22. Oertling, W. A., Surerus, K. K., Einarsdottir, O., Fee, J. A., Dyer, R. B., and Woodruff, W. H. (1994) Spectroscopic characterization of cytochrome ba_3, a terminal oxidase from *Thermus thermophilus*: Comparison of the a_3/CuB site to that of bovine cytochrome aa_3, *Biochemistry 33*, 3128−3141.
23. Than, M. E., and Soulimane, T. (2001) in *Handbook of Metalloproteins* (Messerschmidt, A., Huber, R., Poulos, T., and Wieghardt, K., Eds.) pp 363−378, John Wiley, Chichester, U.K.
24. Giuffrè, A., Forte, E., Antonini, G., D'Itri, E., Brunori, M., Soulimane, T., and Buse, G. (1999) Kinetic properties of ba_3

oxidase from *Thermus thermophilus*: Effect of temperature, *Biochemistry 38*, 1057−1065.
25. Koutsoupakis, K., Stavrakis, S., Pinakoulaki, E., Soulimane, T., and Varotsis, C. (2002) Observation of the equilibrium CuB−CO complex and functional implications of the transient heme a_3 propionates in cytochrome ba_3−CO from *Thermus thermophilus*. Fourier transform infrared (FTIR) and time-resolved step-scan FTIR studies, *J. Biol. Chem. 277*, 32860−32866.
26. Einarsdottir, O., Dyer, R. B., Lemon, D. D., Killough, P. M., Hubig, S. M., Atherton, S. J., Lopez-Garriga, J. J., Palmer, G., and Woodruff, W. H. (1993) Photodissociation and recombination of carbonmonoxy cytochrome oxidase: Dynamics from picoseconds to kiloseconds, *Biochemistry 32*, 12013−12024.
27. Koutsoupakis, C., Soulimane, T., and Varotsis, C. (2003) Ligand binding in a docking site of cytochrome *c* oxidase: A time-resolved step-scan Fourier transform infrared study, *J. Am. Chem. Soc. 125*, 14728−14732.
28. Chien, J. C. W. (1969) Electron paramagnetic resonance study of the stereochemistry of nitrosylhemoglobin, *J. Chem. Phys. 51*, 4220−4227.
29. Dickinson, L. C., and Chien, J. C. W. (1971) Electron paramagnetic resonance study of nitrosylmyoglobin, *J. Am. Chem. Soc. 93*, 5036−5040.
30. Hori, H., Ikeda-Saito, M., and Yonetani, T. (1981) Single-crystal EPR of myoglobin nitroxide. Freezing-induced reversible changes in the molecular orientation of the ligand, *J. Biol. Chem. 256*, 7849−7855.
31. Fago, A., Crumbliss, A. L., Peterson, J., Pearce, L. L., and Bonaventura, C. (2003) The case of the missing NO-hemoglobin: Spectral changes suggestive of heme redox reactions reflect changes in NO-heme geometry, *Proc. Natl. Acad. Sci. U.S.A. 100*, 12087−12092.
32. Kon, H., and Kataoba, N. (1969) Electron paramagnetic resonance of nitric oxide-protoheme complexes with some nitrogenous base. Model systems of nitric oxide hemoproteins, *Biochemistry 8*, 4757−4762.
33. Blokzijl-Homan, M. F. J., and Van Gelder, B. F. (1971) Biochemical and biophysical studies on cytochrome aa_3 III. The EPR spectrum of NO-ferrocytochrome a_3, *Biochim. Biophys. Acta 234*, 493−498.
34. Stevens, T. H., and Chan, S. I. (1981) Histidine is the axial ligand to cytochrome a_3 in cytochrome *c* oxidase, *J. Biol. Chem. 256*, 1069−1071.
35. Stevens, T. H., Bocian, D. F., and Chan, S. I. (1979) EPR studies of ^{15}NO-ferrocytochrome a_3 in cytochrome *c* oxidase, *FEBS Lett. 97*, 314−316.
36. Négrerie, M., Berka, V., Vos, M. H., Liebl, U., Lambry, J.-C., Tsai, A.-L., and Martin, J.-L. (1999) Geminate recombination of nitric oxide to endothelial NO-synthase and mechanistic implications, *J. Biol. Chem. 274*, 24694−24702.
37. Vos, M. H., and Martin, J.-L. (1999) Femtosecond processes in proteins, *Biochim. Biophys. Acta 1411*, 1−20.
38. Pearce, L. L., Bominaar, E. L., Hill, B. C., and Peterson, J. (2003) Reversal of cyanide inhibition of cytochrome *c* oxidase by the auxiliary substrate nitric oxide: An endogenous antidote to cyanide poisoning? *J. Biol. Chem. 278*, 52139−52145.
39. Yoshikawa, S., Shinzawa-Itoh, K., Nakashima, R., Yaono, R., Yamashita, E., Inoue, N., Yao, M., Fei, M. J., Libeu, C. P., Mizushima, T., Yamaguchi, H., Tomizaki, T., and Tsukihara, T. (1998) Redox-coupled crystal structural changes in bovine heart cytochrome *c* oxidase, *Science 280*, 1723−1729.
40. Nitschke, W. (1982) Fe−Ligand Interactions in Myoglobin Single Crystals, Diploma Thesis, University of Regensburg, Germany.
41. Chan, N. L., Kavanaugh, J. S., Rogers, P. H., and Arnone, A. (2004) Crystallographic analysis of the interaction of nitric oxide with quaternary-T human hemoglobin, *Biochemistry 43*, 118−132.
42. Schoot Uiterkamp, A. J. M. (1972) Monomer and magnetic dipole-coupled Cu^{2+} EPR signals in nitrosylhemocyanin, *FEBS Lett. 20*, 93−96.
43. Schoot Uiterkamp, A. J. M., and Mason, H. S. (1973) Magnetic dipole−dipole coupled Cu(II) pairs in nitric oxide-treated tyrosinase: A structural relationship between the active sites of tyrosinase and hemocyanin, *Proc. Natl. Acad. Sci. U.S.A. 70*, 993−996.
44. van Leeuwen, F. X. R., Wever, R., and van Gelder, B. F. (1973) EPR study of nitric oxide-treated reduced ceruloplasmin, *Biochim. Biophys. Acta 315*, 200−203.
45. van Leeuwen, F. X. R., Wever, R., van Gelder, B. F., Avigliano, L., and Mondovi, B. (1975) The interaction of nitric oxide with ascorbate oxidase, *Biochim. Biophys. Acta 403*, 285−291.
46. van Leeuwen, F. X. R., and van Gelder, B. F. (1978) A spectroscopic study of nitric-oxide-treated ceruloplasmin, *Eur. J. Biochem. 87*, 305−312.
47. Boelens, R., Rademaker, H., Pel, R., and Wever, R. (1982) EPR studies of the photodissociation reactions of cytochrome *c* oxidase−nitric oxide complexes, *Biochim. Biophys. Acta 679*, 84−94.
48. Hunter, D. J. B., Salerno, J. C., and Ingledew, W. J. (1998) Angular dependence of electron paramagnetic resonances of an azide−NO complex of cytochrome *c* oxidase: Orientation of the haem-copper axis in cytochrome aa_3 from ox heart, *Biochim. Biophys. Acta 1364*, 55−62.
49. Boas, J. F., Dunhill, R. H., Pilbrow, J. R., Srivastava, R. C., and Smith, T. D. (1969) Electron spin resonance studies of copper (II) hydroxy- carboxylic acid chelates in aqueous and non-aqueous solutions, *J. Chem. Soc. A 94*, 94−108.
50. Arciero, D. M., Orville, A. M., and Lipscomb, J. D. (1985) [^{17}O]-Water and nitric oxide binding by protocatechuate 4,5-dioxygenase and catechol 2,3-dioxygenase. Evidence for binding of exogenous ligands to the active site Fe^{2+} of extradiol dioxygenases, *J. Biol. Chem. 260*, 14035−14044.
51. Jackson, T. A., Yikilmaz, E., Miller, A. F., and Brunold, T. C. (2003) Spectroscopic and computational study of a non-heme iron $\{Fe-NO\}^7$ system: Exploring the geometric and electronic structures of the nitrosyl adduct of iron superoxide dismutase, *J. Am. Chem. Soc. 125*, 8348−8363.
52. Ruggiero, C. E., Carrier, S. M., Antholine, W. E., Whittaker, J. W., Cramer, C. J., and Tolman, W. B. (1993) Synthesis and structural and spectroscopic characterization of mononuclear copper nitrosyl complexes: Models for nitric oxide adducts of copper proteins and copper-exchanged zeolites, *J. Am. Chem. Soc. 115*, 11285−11298.
53. Tsukihara, T., Aoyama, H., Yamashita, E., Tomizaki, T., Yamaguchi, H., Shinzawa-Itoh, K., Nakashima, R., Yaono, R., and Yoshikawa, S. (1996) The whole structure of the 13-subunit oxidized cytochrome *c* oxidase at 2.8 Å, *Science 272*, 1136−1144.
54. Ostermeier, C., Harrenga, A., Ermler, U., and Michel, H. (1997) Structure at 2.7 Å resolution of the *Paracoccus denitrificans* two-subunit cytochrome *c* oxidase complexed with an antibody FV fragment, *Proc. Natl. Acad. Sci. U.S.A. 94*, 10547−10553.
55. Svensson-Ek, M., Abramson, J., Larsson, G., Tornroth, S., Brzezinski, P., and Iwata, S. (2002) The X-ray crystal structures of wild-type and EQ(I-286) mutant cytochrome *c* oxidases from *Rhodobacter sphaeroides*, *J. Mol. Biol. 321*, 329−339.
56. Chao, C.-C., and Lunsford, J. H. (1974) Infrared and electron paramagnetic resonance study of some silver-nitric oxide complexes in Y type zeolites, *J. Phys. Chem. 78*, 1174−1177.
57. Giamello, E., Murphy, D., Magnacca, G., Morterra, C., Anpo, M., Nomura, T., and Shyoya, Y. (1992) The interaction of NO with copper ions in ZSM5. An EPR and IR investigation, *J. Catal. 136*, 510.
58. Tocheva, E. I., Rosell, F. I., Mauk, A. G., and Murphy, M. E. P. (2004) Side-on copper-nitrosyl coordination by nitrite reductase, *Science 304*, 867−870.
59. Sayle, R. A., and Milner-White, E. J. (1995) RASMOL: Biomolecular graphics for all, *Trends Biochem. Sci. 20*, 374−376.

BI0488808